JOURNAL OF MAGNETIC RESONANCE **135,** 1–13 (1998)
ARTICLE NO. MN981534

Model-Free Analysis of Stretched Relaxation Dispersions

Bertil Halle,[1] Haukur Jóhannesson, and Kandadai Venu[2]

Department of Chemistry, Condensed Matter Magnetic Resonance Group, Lund University, P.O. Box 124, S-22100 Lund, Sweden

E-mail: bertil.halle@fkem2.lth.se.

Received December 22, 1997; revised June 9, 1998

Nuclear magnetic relaxation dispersion (NMRD) measurements can provide valuable information about the dynamics and structure of macromolecular solutions and other complex fluids. A large number of ^{1}H NMRD studies of water in concentrated protein solutions and in semisolid biological samples have been reported. The observed dispersion usually extends over a wide frequency range and then cannot be described by a Lorentzian spectral density function. We propose here a model-free approach for analyzing such stretched dispersion profiles. Unlike the traditional empirical fitting procedures, the model-free approach is based on rigorous theory and produces parameters with well-defined physical significance. The model-free approach is validated with the aid of synthetic relaxation data, showing that it is robust and accurate, and is then applied to new water ^{1}H NMRD data from solutions of the protein bovine pancreatic trypsin inhibitor (BPTI). By separating the static and dynamic information content of the relaxation dispersion, the model-free analysis shows that the dramatic salt effect observed in BPTI solutions is due almost entirely to a slowing down of protein rotation with little change of protein structure. An analysis of the same data in terms of the empirical dispersion function used in most ^{1}H NMRD studies leads to a qualitatively different picture. We demonstrate that this widely used dispersion function is unphysical and that its parameters do not have the physical meaning usually ascribed to them.

Key Words: **relaxation dispersion; NMRD; model-free analysis; protein association; BPTI.**

INTRODUCTION

Within the motional-narrowing regime, all information about molecular motions that can be derived from nuclear spin relaxation rates is contained in the spectral density function (*1*). To map out the frequency dependence of this function, the relaxation rate must be measured over a wide range of magnetic field strengths. Such *n*uclear *m*agnetic *r*elaxation *d*ispersion (NMRD) measurements can be carried out with fast field-cycling techniques (*2*) or with tunable and fixed-field spectrometers of conventional type (*3*). Most NMRD studies reported to date have been concerned with the relaxation of the water ^{1}H (and more recently, ^{2}H and ^{17}O) resonance in biological systems ranging in complexity from dilute protein solutions to intact tissue (*4, 5*). For relatively dilute protein solutions, the dispersion is generally found (*5*) to be of Lorentzian form, as expected for relaxation induced by rotational diffusion of nearly spherical noninteracting proteins. The first water ^{1}H relaxation dispersion profiles to be reported from protein solutions (*6–8*), however, extended over a much wider frequency range than a Lorentzian dispersion (see Fig. 1). Subsequent water ^{1}H NMRD studies of biopolymer solutions, gels, and tissues have shown that such a stretched dispersion shape is the rule rather than the exception (*4, 9–29*).

Qualitatively, it is clear that dispersion stretching can have several causes, including complex protein reorientational dynamics (due to structural heterogeneity induced by protein–protein interactions), a distribution of proton exchange rates (for buried water molecules and labile protein protons), or a distribution of intermolecular dipole couplings (for immobilized proteins) (*3*). The quantitative analysis of stretched water ^{1}H dispersion profiles, however, is nontrivial. Two principal approaches have been tried. In one, the dispersion shape follows from a microscopic model, the parameters of which are determined from a direct fit to the dispersion data. Unless the origin of dispersion stretching is well understood, however, the physical significance of the derived parameters is questionable. The other approach is an empirical one, where the dispersion data are parametrized by a convenient and physically plausible mathematical function. The vast majority of water ^{1}H dispersions have been analyzed by an empirical 3-parameter function known as "the Cole–Cole expression" (*4, 9, 17*). Although this function has no a priori validity, the parameters are generally interpreted as if they had a definitive physical significance. In particular, the characteristic time derived from the frequency where the dispersion has decayed to half its maximum amplitude is interpreted as a rotational correlation time.

In the present work, we examine this empirical dispersion function and find that it is fundamentally inconsistent and may lead to qualitatively incorrect inferences about the behavior of the investigated system. We then describe a model-free approach to the analysis of stretched dispersion profiles, which

[1] To whom correspondence should be addressed.

[2] Current address: School of Physics, University of Hyderabad, Hyderabad, 500046, India.

1090-7807/98 $25.00

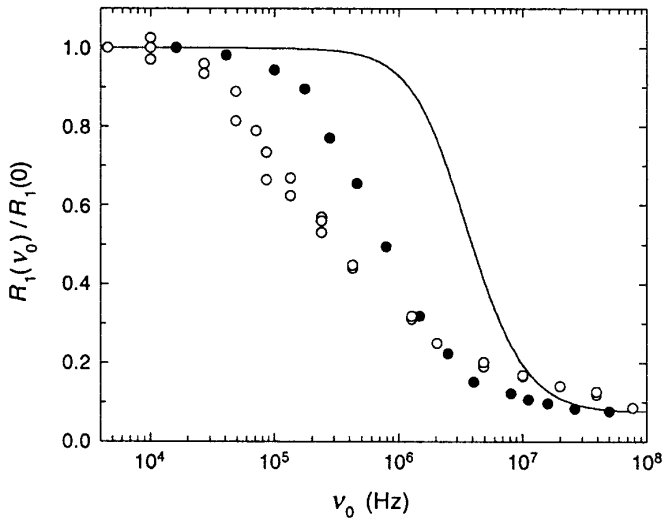

FIG. 1. Dispersion of the water ^{1}H longitudinal relaxation rate R_1 in aqueous solutions of 15 weight% human apotransferrin at 298 K (●) (*6*) and 28 weight% bovine serum albumin at 303 K (○) (*8*). The relaxation rate is normalized by the measured rate at the lowest frequency (10.8 s^{-1} for apotransferrin and 20.0 s^{-1} for serum albumin). The curve is a Lorentzian dispersion with a correlation time of 25 ns, as expected for the tumbling of these proteins in dilute solution.

we argue is preferable to both empirical analysis and multiparameter model fitting. In the model-free approach, the quantities extracted from the dispersion data have a well-defined physical significance and do not rely on any model assumptions. With the aid of synthetic dispersion data, we demonstrate that the model-free analysis is robust and accurate. We then present new water ^{1}H dispersion data from BPTI solutions, revealing a dramatic salt effect. These data are analyzed by the model-free approach and by the empirical "Cole–Cole" approach. The parameter values derived by these two approaches differ greatly and even lead to qualitatively different conclusions regarding the origin of the salt effect.

FUNDAMENTALS

The nuclear spin relaxation rate becomes frequency-dependent when the motional frequencies modulating the spin–lattice coupling are comparable to the level spacings of the spin system (*1*). Within the motional-narrowing regime, the effect of a fluctuating (classical) lattice variable $V(t)$ on the spin relaxation behavior can be fully described in terms of the time correlation function (TCF)

$$C(\tau) = \langle V(t)^* V(t+\tau)\rangle. \qquad [1]$$

The TCF is a real-valued quantity and, for dynamic models obeying the detailed balance condition, is invariant under time reversal:

$$C(-\tau) = C(\tau). \qquad [2]$$

The relaxation superoperator involves the complex-valued spectral density function (SDF)

$$Z(\omega) = \int_0^\infty d\tau \exp(-i\omega\tau) C(\tau), \qquad [3]$$

which may be decomposed as

$$Z(\omega) = J(\omega) - iK(\omega). \qquad [4]$$

The real part of $Z(\omega)$ is the usual SDF,

$$J(\omega) = \int_0^\infty d\tau \cos(\omega\tau) C(\tau), \qquad [5]$$

that determines the spin relaxation rates. For dipolar relaxation of a like-spin pair (*1*) and for quadrupolar relaxation in the effectively exponential regime (*30*), the longitudinal relaxation rate R_1 depends on the resonance frequency ω_0 according to

$$R_1 = \omega_{RL}^2 [0.2\, J(\omega_0) + 0.8\, J(2\omega_0)], \qquad [6]$$

where ω_{RL} is the (dipolar or quadrupolar) rigid-lattice coupling frequency. The imaginary part of $Z(\omega)$,

$$K(\omega) = \int_0^\infty d\tau \sin(\omega\tau) C(\tau), \qquad [7]$$

gives rise to the dynamic shift (*31*), which can affect the lineshape but not the longitudinal relaxation.

Certain simple dynamic models, such as spherical-top rotational diffusion in an isotropic medium, lead to an exponential TCF,

$$C(\tau) = C(0)\exp(-|\tau|/\tau_C), \qquad [8]$$

and, hence, to a Lorentzian SDF,

$$J(\omega) = C(0)\,\frac{\tau_C}{1 + (\omega\tau_C)^2}. \qquad [9]$$

In this simple case, the relaxation dispersion $R_1(\omega_0)$ provides two distinct pieces of information about the investigated system: $C(0)$ and τ_C. The initial TCF is the mean-square fluctuation of the lattice variable, $C(0) = \langle |V|^2\rangle$; it contains information about the equilibrium structure of the system but is entirely independent of the dynamics. The correlation time τ_C,

on the other hand, is a purely dynamic quantity that provides the time scale for thermal randomization of the lattice variable $V(t)$ (usually a function of molecular orientation).

In concentrated macromolecular solutions and other complex fluids, the TCF usually decays nonexponentially. This may be due to heterogeneity at the molecular level, as may result from protein association, or to collective motions involving many coupled degrees of freedom, e.g., the undulation of phospholipid bilayer membranes. In either case, the decay of the TCF is slower than exponential and, hence, the decay of the SDF is stretched out over a wider frequency range than for a Lorentzian SDF. If the structural and dynamic complexities can be adequately modeled, it may be possible to determine the model parameters from a fit to the relaxation dispersion. In many cases, however, the functional form of the SDF is not known a priori. A nontrivial problem then arises: How should the stretched dispersion profile be analyzed? In other words: What, if any, unique information about the system can be extracted from the relaxation data?

EMPIRICAL DISPERSION FUNCTIONS

Dielectric Relaxation

The problem of stretched dispersions was first encountered in the dielectric relaxation of amorphous solids and viscous liquids (*32, 33*). The observable here is the frequency-dependent complex dielectric constant $\epsilon^*(\omega)$, conventionally decomposed as

$$\epsilon^*(\omega) = \epsilon'(\omega) - i\epsilon''(\omega). \qquad [10]$$

The real (in-phase) part, $\epsilon'(\omega)$, is the (relative) dielectric permittivity and the imaginary (90° phase-shifted) part, $\epsilon''(\omega)$, is the dielectric loss factor. The frequency dependencies of $\epsilon'(\omega)$ and $\epsilon''(\omega)$ are usually referred to as dielectric dispersion and dielectric absorption, respectively, in analogy with the corresponding optical phenomena. There is also a complete analogy with the dispersion and absorption components of the free induction decay in magnetic resonance. In all these cases, the dispersion and absorption components are linked by the Kramers–Kronig relations, which follow directly from the linearity and causality of the response of the system to a weak harmonic perturbation (*34*).

Since polar molecules are much more strongly coupled than are nuclear spins, the theory of dielectric relaxation is more complicated. If dipole–dipole correlations are neglected, however, $\epsilon^*(\omega)$ can be related to the electric–dipole TCF as (*35*)

$$\epsilon^*(\omega) - \epsilon_0 = -i\omega Z(\omega), \qquad [11]$$

where ϵ_0 is the static relative permittivity and the complex dipolar SDF $Z(\omega)$ is related to the electric–dipole TCF $C(\tau)$ as in Eq. [3]. It then follows from Eqs. [4] and [10] that

$$\epsilon'(\omega) - \epsilon_0 = -\omega K(\omega), \qquad [12a]$$

$$\epsilon''(\omega) = \omega J(\omega). \qquad [12b]$$

In Debye's theory of dielectric relaxation (*36*), isotropic rotational diffusion leads to an exponential TCF of the same form as Eq. [8], with $C(0) = \epsilon_0 - \epsilon_\infty$ and τ_C identified as the Debye rotational relaxation time. Consequently,

$$\epsilon'(\omega) - \epsilon_\infty = C(0)\,\frac{1}{1 + (\omega\tau_C)^2}, \qquad [13a]$$

$$\epsilon''(\omega) = C(0)\,\frac{\omega\tau_C}{1 + (\omega\tau_C)^2}. \qquad [13b]$$

The standard approach for analyzing the frequency-dependent dielectric response from non-Debye materials is to invoke a continuous distribution, $f(\tau_C)$, of correlation times, i.e., the TCF is expressed as

$$C(\tau) = C(0)\int_0^\infty d\tau_C\, f(\tau_C)\exp(-|\tau|/\tau_C). \qquad [14]$$

The simplest version of this empirical approach is to use a two-parameter distribution function with a characteristic time τ_0 and a dimensionless width parameter. The first function of this kind to be introduced was the so-called log-normal distribution (*32, 33*),

$$f(\tau_C) = \frac{1}{\tau_C\sqrt{2\pi\sigma^2}}\exp\left\{-\frac{1}{2}\left[\frac{1}{\sigma}\ln\left(\frac{\tau_C}{\tau_0}\right)\right]^2\right\}. \qquad [15]$$

This is a skewed distribution, where the average correlation time, $\langle\tau_C\rangle = \tau_0\exp(\sigma^2/2)$, exceeds the most probable correlation time, $\hat{\tau}_C = \tau_0\exp(-\sigma^2)$. The width parameter σ can be interpreted as the root-mean-square variation of the activation enthalpy (in units of k_BT) for a process with a jump rate describable by transition-state theory. The SDFs $J(\omega)$ and $K(\omega)$ resulting from a log-normal τ_C distribution have to be evaluated numerically.

A compact analytical representation with the same number of parameters (one more than in the Debye model) was introduced by Cole and Cole (*37*),

$$\epsilon^*(\omega) - \epsilon_\infty = C(0)\,\frac{1}{1 + (i\omega\tau_0)^b}, \qquad [16]$$

where the positive exponent b (≤ 1) measures the degree of stretching of the dispersion with respect to the Debye case ($b = 1$). Combination of Eqs. [10], [12], and [16] yields for the SDFs

$$J(\omega) = -C(0)\,\frac{1}{\omega}\,\mathrm{Im}\left[\frac{1}{1+(i\omega\tau_0)^b}\right]$$
$$= C(0)\,\frac{1}{\omega}\,\frac{(\omega\tau_0)^b\sin(b\pi/2)}{1+2(\omega\tau_0)^b\cos(b\pi/2)+(\omega\tau_0)^{2b}}, \quad [17a]$$

$$K(\omega) = C(0)\,\frac{1}{\omega}\,\mathrm{Re}\left[\frac{1}{1+(i\omega\tau_0)^{-b}}\right]. \quad [17b]$$

The empirical Cole–Cole function describes dielectric relaxation data from a variety of systems with remarkable accuracy. Yet, it has no a priori validity and is therefore nothing more than a convenient representation of the data.

If the system can be modeled in terms of a continuous distribution of correlation times, then the SDF $J(\omega)$ corresponding to the TCF in Eq. [14] is

$$J(\omega) = C(0)\int_0^\infty d\tau_C\, f(\tau_C)\,\frac{\tau_C}{1+(\omega\tau_C)^2}. \quad [18]$$

Fuoss and Kirkwood showed that this integral transform can be inverted analytically (*38*):

$$f(\tau_C) = -\frac{2}{\pi\tau_C^2}\,\mathrm{Im}[J(\omega = i/\tau_C)]. \quad [19]$$

In principle, this result would allow a unique τ_C distribution to be extracted from experimental dispersion data. In practice, however, numerical difficulties severely limit the usefulness of the inversion formula. Nevertheless, it can be used to calculate the τ_C distribution corresponding to any integrable analytic function $J(\omega)$. For example, the Cole–Cole SDF in Eq. [17a] corresponds to the distribution function (*37*)

$$f(\tau_C) = \frac{1}{2\pi\tau_C}\,\frac{\sin(b\pi)}{\cos(b\pi)+\cosh[b\,\ln(\tau_C/\tau_0)]}. \quad [20]$$

Nuclear Spin Relaxation

Many of the results first derived in a dielectric context can be directly carried over to nuclear spin relaxation. The initial motivation for invoking correlation time distributions in NMR, however, was not to analyze stretched dispersions but to account for an unexpected temperature dependence of T_1 and T_2 for polymers and adsorbed water. The log-normal distribution was thus used to rationalize anomalies in the T_1/T_2 ratio and in the temperature dependence of T_1 near the temperature of the T_1 minimum (*39–45*). The Cole–Cole SDF in Eq. [17a] has also been used in this connection (*39, 42*).

The earliest reported relaxation dispersion profiles (*6–8*), of the water ^{1}H resonance in concentrated protein solutions, were distinctly stretched and could not be adequately described by a Lorentzian SDF (see Fig. 1). The log-normal distribution was used to analyze some of these early dispersion profiles (*7, 8, 46*), but the physical significance of the parameters in this empirical distribution remained obscure.

While the Cole–Cole distribution has been used to analyze the anomalous temperature dependence of T_1 and T_2 (*39, 42*), it has not, and cannot, be used to describe relaxation dispersion profiles. Like the log-normal distribution [15], the Cole–Cole distribution [20] is skewed towards long correlation times (but is symmetric on a logarithmic scale). The wings of the Cole–Cole distribution, however, decay so slowly, asymtotically as $(\tau_C)^{-(b+1)}$, that the first moment of the distribution diverges. This is most readily seen from Eqs. [17] and [18]. Setting $\omega = 0$ in Eq. [18], we obtain the general result

$$J(0) = C(0)\langle\tau_C\rangle. \quad [21]$$

Taking the limit $\omega \to 0$ of Eq. [17a], however, we find that $J(0) \sim \omega^{b-1} \to \infty$ for $b < 1$. This is evidently due to the divergence of $\langle\tau_C\rangle$. While a τ_C distribution with a divergent first moment is not necessarily unphysical, a divergent relaxation rate surely is. Within the context of nuclear spin relaxation, a divergent SDF indicates that the motional-narrowing condition is violated and, hence, that a more general theory of spin relaxation must be used (*1*). This difficulty does not appear in the dielectric context because the measured dielectric response is related to the Fourier transform of the time derivative of the TCF, rather than of the TCF itself. This gives rise to the ω factor in Eqs. [11] and [12], which removes the divergence.

The Hallenga–Koenig Function

A very large number of ^{1}H NMRD studies have been performed on water in biological and colloidal systems, ranging from macromolecular solutions to gels and tissues. The dispersion is nearly always found to be stretched out over a wider frequency range than predicted by the Lorentzian SDF in Eq. [9]. The vast majority of these stretched dispersion profiles have been analyzed in terms of an empirical dispersion function refered to as "the Cole–Cole expression" (*4, 9–29*). First introduced by Hallenga and Koenig, this empirical function takes the form (*9*)

$$J(\omega) = A\,\mathrm{Re}\left[\frac{1}{1+(i\omega\tau_0)^\kappa}\right]$$
$$= A\,\frac{1+(\omega\tau_0)^\kappa\cos(\kappa\pi/2)}{1+2(\omega\tau_0)^\kappa\cos(\kappa\pi/2)+(\omega\tau_0)^{2\kappa}}. \quad [22]$$

In addition, one usually introduces the highly accurate (*6*), but unnecessary, approximation of replacing the linear combination $0.2\,J(\omega_0) + 0.8\,J(2\omega_0)$ in Eq. [6] by $J(\sqrt{3}\,\omega_0)$. Like the

Cole–Cole function in Eq. [17a], the Hallenga–Koenig (HK) function [22] reduces to the Lorentzian SDF [9] in the trivial limit $\kappa = 1$ if one identifies A with $C(0)\ \tau_C$. Furthermore, for any κ value in the allowed range $0 < \kappa \leq 1$, the HK function drops to half its maximum value at $\omega = 1/\tau_0$, as does a Lorentzian SDF at $\omega = 1/\tau_C$. (These frequencies also define the inflection points of the dispersion profiles when plotted on a logarithmic frequency scale.)

It was acknowledged at the outset that the HK function has no a priori validity (*9*). Yet, the parameters A and τ_0 extracted from fits to dispersion data are generally assigned definite physical meanings and quantitatively compared to other data. (Apparently, no attempt has been made to physically interpret the parameter κ.) In particular, when water relaxation dispersions from protein solutions are analyzed, τ_0 is always identified with the rotational correlation time of the protein.

It has frequently been stated (*4, 9–11, 17, 21, 22, 29*), and is apparently widely believed, that Eq. [22] is the direct analogue of the Cole–Cole dispersion used to analyze dielectric relaxation data and, therefore, that the two expressions have the same physical basis. A comparison of Eqs. [17] and [22], however, shows that the HK function differs in important ways from the Cole–Cole function. Furthermore, despite claims to the contrary (*4, 17*), the HK function does not satisfy the Kramers–Kronig relation, as required for any physically admissible SDF (*1*).

The Kramers–Kronig relation expresses a general connection between the in-phase (dispersion) and 90° out-of-phase (absorption) linear response of a causal system (*34*). In our notation, it takes the form

$$K(\omega) = \frac{2\omega}{\pi} \int_0^\infty d\omega' \, \frac{J(\omega')}{\omega^2 - (\omega')^2}. \qquad [23]$$

Since

$$\frac{2\omega}{\pi} \int_0^\infty d\omega' \, \frac{\cos(\omega'\tau)}{\omega^2 - (\omega')^2} = \sin(\omega\tau),$$

it is clear that any pair of SDFs $J(\omega)$ and $K(\omega)$ derived from a TCF $C(\tau)$ by cosine and sine transforms, as in Eqs. [5] and [7], satisfies the Kramers–Kronig relation. Since the Cole–Cole functions in Eq. [17] can be so derived (from an exponential TCF averaged over the τ_C distribution [20]), they must therefore satisfy the Kramers–Kronig relation. The HK function with $\kappa < 1$, however, cannot be derived from any physically admissible TCF. This follows directly from a general condition on the SDF of a stationary random variable $V(t)$, namely that the integral of $J(\omega)$ over all frequencies is proportional to the mean-square fluctuation $\langle |V|^2 \rangle$. Using the time-reversal invariance in Eq. [2], we can express Eq. [5] as

$$J(\omega) = \frac{1}{2} \, \mathrm{Re} \int_{-\infty}^\infty d\tau \, \exp(-i\omega\tau) C(\tau). \qquad [24]$$

By integrating both members of this equation over ω, interchanging the order of integration, and recognizing the Fourier integral representation of the delta function, $2\pi\delta(\tau) = \int_{-\infty}^{\infty} d\omega \exp(-i\omega\tau)$, we obtain

$$\int_0^\infty d\omega \, J(\omega) = \frac{\pi}{2} \, C(0). \qquad [25]$$

The integral of the HK function [22], however, is divergent for $\kappa < 1$ since $J(\omega) \sim \omega^{-\kappa}$ asymptotically. In fact,

$$\int_0^\infty d\omega \, J(\omega) = \frac{\pi}{2} \frac{A}{\tau_0^\kappa} \, \mathrm{sinc}[(1 - \kappa)\pi/2] \lim_{\omega \to \infty} \omega^{1-\kappa}. \qquad [26]$$

In the Lorentzian limit, $\kappa = 1$, this yields with Eq. [25], $A = C(0)\ \tau_0$, as expected. For $\kappa < 1$, however, the integral diverges and, since $C(0) = \langle |V|^2 \rangle$ must be finite, it follows that the HK function is unphysical for $\kappa < 1$.

MODEL-FREE ANALYSIS

General Principles

If empirical dispersion functions (whether unphysical or not) are dismissed, what sense can then be made of stretched relaxation dispersion data when the system is not sufficiently well understood to formulate a realistic model? If the range of the dispersion data is wide enough to define the low- and high-frequency plateaus reasonably well, several rigorously defined physical quantities can actually be extracted without invoking a model. One such quantity is the integral of the dispersion profile, which, according to Eq. [25], yields the mean-square fluctuation

$$C(0) = \frac{2}{\pi} \int_0^\infty d\omega \, J(\omega). \qquad [27]$$

The natural definition of an "average" motional time scale associated with a stretched dispersion is the time integral of the reduced TCF,

$$\langle \tau_C \rangle = \int_0^\infty d\tau \, C(\tau)/C(0) = J(0)/C(0), \qquad [28]$$

obtained from the low-frequency dispersion plateau $J(0)$ and

the dispersion integral. For a heterogeneous system with a spatial distribution of isotropic rotational correlation times, $\langle\tau_C\rangle$ in Eq. [28] is simply the population-weighted average, as in Eq. [21]. If the nonexponentiality of $C(\tau)$ reflects collective motions, $\langle\tau_C\rangle$ is an average of mode correlation times weighted by the corresponding mode amplitudes.

The approach described here has some important advantages over conventional strategies for analyzing stretched dispersions. First, the quantities $C(0)$ and $\langle\tau_C\rangle$ are rigorously defined in terms of the fundamental TCF and therefore have well-defined physical significance. This is not the case for the parameters A and τ_0 in the HK function. Second, the present analysis separates the static and dynamic aspects of the information content. In particular, the mean-square fluctuation $C(0)$ is rigorously independent of the dynamics, i.e., the rates of molecular motions. As illustrated under Applications, this separation of information can provide important clues about the physical mechanism responsible for a stretched dispersion. Third, the quantities $C(0)$ and $\langle\tau_C\rangle$ are model-independent and therefore not biased by any unproven mechanistic assumptions. In contrast, a direct multiparameter fit to a stretched dispersion provides nonunique results that stand and fall with the legitimacy of the assumed model. A complete interpretation of the data, of course, requires that a model be introduced at some stage. The approach we advocate is to first determine the model-free quantities $C(0)$ and $\langle\tau_C\rangle$, which have indisputable physical significance, and further interpret these quantities only when and if a realistic model can be formulated. Having isolated the purely static information content of the dispersion in the form of $C(0)$ is then a decisive advantage, because the static (structural) features of a complex system are usually far easier to model than the dynamic ones.

While a Lorentzian dispersion is fully characterized by two parameters, a stretched dispersion contains more information. In many cases, such as water ^{1}H NMRD data from macromolecular solutions, the dispersion can be adequately represented by 3 or 4 parameters. In addition to the quantities $C(0)$ and $\langle\tau_C\rangle$, it should therefore be possible to extract one or two independent measures of dispersion shape. Model-independent shape indicators can be defined in many ways. A reasonable approach is to characterize the shape of a stretched dispersion $J(\omega)$ with reference to a Lorentzian $J_0(\omega)$ with the same low- and high-frequency limits as $J(\omega)$ and with the same frequency at half amplitude. The inverse of this frequency defines a characteristic time τ_0 that can be obtained from the condition

$$J(\omega = 1/\tau_0) = \tfrac{1}{2}\, J(0). \qquad [29]$$

The Lorentzian

$$J_0(\omega) = \frac{J(0)}{1 + (\omega\tau_0)^2} \qquad [30]$$

thus intersects $J(\omega)$ at the frequency $\omega = 1/\tau_0$, where both SDFs have decayed to half of the low-frequency limit $J(0)$. It follows from Eqs. [27], [28], and [30] that

$$\frac{\tau_0}{\langle\tau_C\rangle} = \int_0^\infty d\omega\; J(\omega) \Bigg/ \int_0^\infty d\omega\; J_0(\omega). \qquad [31]$$

With τ_0 defined as in Eq. [29], the integral of $J(\omega)$ is generally larger than that of the reference Lorentzian, so that $\tau_0 \geq \langle\tau_C\rangle$.

The asymmetry of a stretched dispersion $J(\omega)$ relative to the reference Lorentzian $J_0(\omega)$ may be characterized by the two quantities

$$\lambda_- = 2 \int_0^{1/\tau_0} \frac{d\omega}{\omega}\, [\, J_0(\omega) - J(\omega)/J(0), \qquad [32a]$$

$$\lambda_+ = 2 \int_{1/\tau_0}^\infty \frac{d\omega}{\omega}\, [\, J(\omega) - J_0(\omega)]/J(0. \qquad [32b]$$

In a plot of $J(\omega)/J(0)$ versus $\ln\omega$, $\lambda_-/2$ and $\lambda_+/2$ are the areas of the two regions bounded by $J(\omega)$ and $J_0(\omega)$ below and above their intersection, respectively (see Fig. 2a).

Numerical Implementation

To determine the model-free parameters $C(0)$, $\langle\tau_C\rangle$, τ_0, and $\lambda_\pm$, a discrete set of noisy data points must be integrated. This calls for interpolation and smoothing, which may be accomplished in many ways. One possibility, which we have found useful, is to introduce a continuous interpolation function that represents the data to an accuracy commensurate with the measurement error. The functional form should be physically plausible and capable of representing most experimental dispersion profiles with a small number of parameters (compared to the number of data points). The natural choice is the multi-Lorentzian form

$$J(\omega) = \sum_{n=1}^{N} c_n \frac{\tau_n}{1 + (\omega\tau_n)^2}, \qquad [33]$$

which can represent the SDF of any stationary Markov process $V(t)$ obeying detailed balance (*47*). This covers virtually all cases of interest, including fast exchange processes among discrete states or sites in a heterogeneous system (described by a discrete master equation) and all types of single-particle or collective dynamics governed by a Fokker–Planck equation, e.g., free rotational diffusion of an asymmetric-top rotor (*48*), restricted rotational diffusion (*49*), translational diffusion on curved surfaces (*50*), and collective director fluctuations (*51*).

The $2N$ parameters of the multi-Lorentzian representation

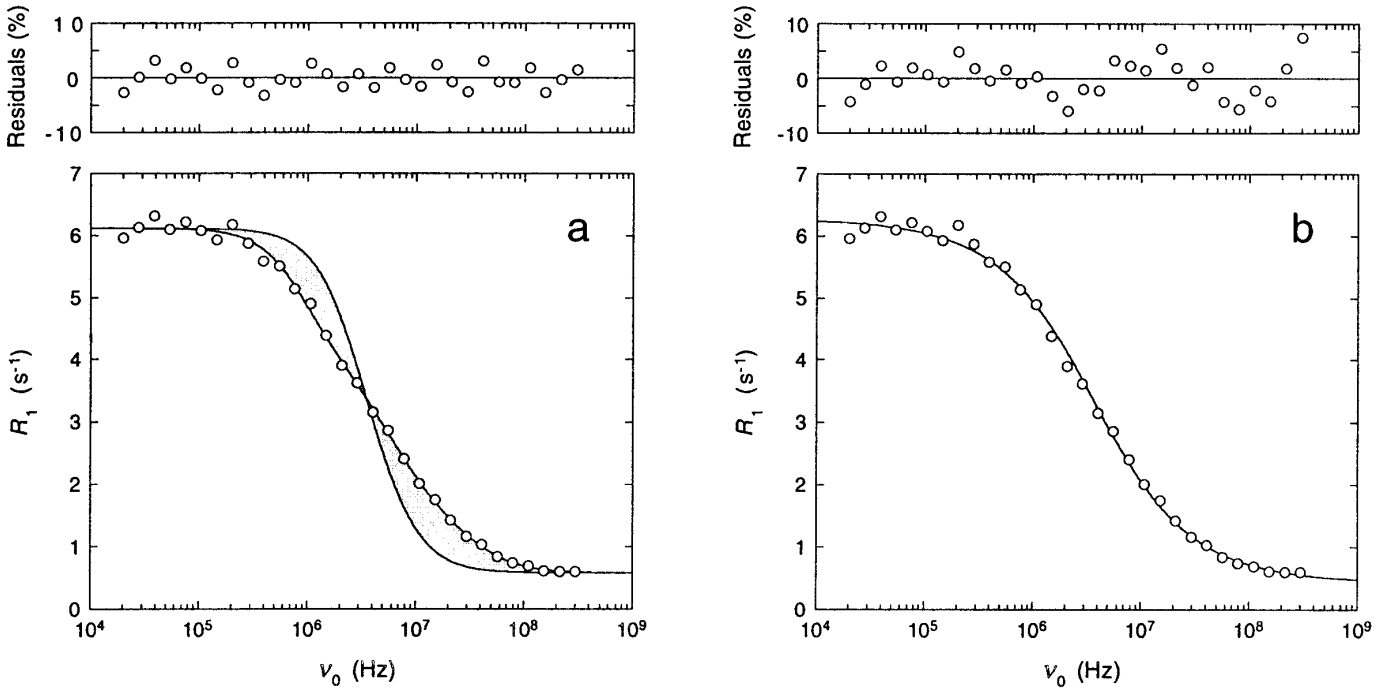

FIG. 2. Synthetic relaxation dispersion data analyzed with the model-free approach (a) and the HK approach (b). A Lorentzian dispersion with the same frequency at half amplitude as the fitted dispersion curve is also shown in (a). The shaded areas are proportional to the shape parameters λ_- and λ_+.

[33] can be determined by any nonlinear parameter estimation method, e.g., the Levenberg–Marquardt algorithm (*52*). This numerical problem is analogous to multiexponential decomposition of a decaying signal, such as the free induction decay, and has been amply discussed (*53*). The number N of Lorentzians to be included can be objectively determined by means of the F test (*52*). A fit of N Lorentzian terms to M data points $J(\omega_i)$ with errors σ_i yields the reduced chi-square merit function

$$\chi_r^2(N) = \frac{1}{(M-2N)} \sum_{i=1}^{M} \frac{1}{\sigma_i^2} \left[J(\omega_i) - \sum_{n=1}^{N} \frac{c_n \tau_n}{1 + (\omega_i \tau_n)^2} \right]^2. \quad [34]$$

Another fit is then made with $N + 1$ Lorentzians, yielding $\chi_r^2(N+1)$, and if the fit was substantially improved the ratio $F = \chi_r^2(N)/\chi_r^2(N+1)$ will be large. If the measurement errors are normally distributed, the quantity F follows the F distribution and the probability of observing a smaller F value is $P(N+1) = 1 - I_\mu((M-2N-2)/2, (M-2N)/2)$, with $I_\mu(a,b)$ the incomplete beta function and $\mu = \chi_r^2(N+1)/[\chi_r^2(N) + \chi_r^2(N+1)]$. The additional Lorentzian term is accepted only if this probability exceeds a preassigned cutoff value, P_0. With $P_0 = 0.90$, for example, a fourth Lorentzian term requires a 2.5-fold reduction of χ_r^2 for 20 data points but only a 34% reduction for 100 points. Starting with $N = 1$ and successively adding terms until $P(N+1) < P_0$, we can thus construct an optimal N-Lorentzian representation of the data in a well-defined way.

The multi-Lorentzian representation has the further appeal of being analytically integrable. Substituting Eq. [33] into Eqs. [27]–[29] and [32], we obtain

$$C(0) = \sum_n c_n, \quad [35]$$

$$\langle \tau_C \rangle = \sum_n c_n \tau_n \Big/ \sum_n c_n, \quad [36]$$

$$\lambda_\pm = \sum_n c_n \tau_n \ln\{\tfrac{1}{2}[1 + (\tau_0/\tau_n)^{\pm 2}]\} \Big/ \sum_n c_n, \quad [37]$$

with τ_0 determined by the implicit relation

$$\sum_n \frac{c_n \tau_n}{1 + (\tau_n/\tau_0)^2} = \tfrac{1}{2} \sum_n c_n \tau_n. \quad [38]$$

For small deviations from Lorentzian shape, $\tau_0 = \langle \tau_C^2 \rangle / \langle \tau_C \rangle$, which always is $\geq \langle \tau_C \rangle$, and $\lambda_- + \lambda_+ = \langle \tau_C \rangle \langle \tau_C^3 \rangle / \langle \tau_C^2 \rangle^2 - 1$, with $\langle \tau_C^k \rangle = \Sigma_n c_n \tau_n^k / \Sigma_n c_n$.

The multi-Lorentzian fit provides error estimates for the $2N$ parameters $\{c_n, \tau_n\}$, but these errors are not independent and therefore not suitable for estimating the errors in the model-free parameters. The latter can be rigorously calculated by the

Monte Carlo method (*52*). In this method, the $\{c_n,\tau_n\}$ obtained from a fit are regarded as the true values of these parameters. A synthetic data set $J(\omega_i)$, $i = 1,2, \ldots, M$, is then generated by computing each $J(\omega_i)$ from Eq. [33] with the "true" parameter values and adding a "measurement error" by generating a random number from a normal distribution, the variance of which is determined by the actual measurement error σ_i. A fit to these synthetic data yields a new parameter set $\{c_n,\tau_n\}$, from which the model-free parameters are calculated according to Eqs. [35]–[38]. By repeating this procedure many times, one obtains an ensemble of values for each model-free parameter, from which the error at a given confidence level can readily be obtained.

We emphasize that the parameters $\{c_n,\tau_n\}$ should not, in general, be ascribed physical significance. The multi-Lorentzian representation is merely a convenient mathematical device used in an intermediate step of the model-free analysis. Only if independent information suggests that the system can actually be modeled by a fixed number of Lorentzians should a direct physical interpretation of the parameters $\{c_n,\tau_n\}$ be attempted.

APPLICATIONS

In this section, the model-free approach is first validated by analyzing synthetic relaxation dispersion data and then applied to new ^{1}H NMRD data from solutions of the well-studied 6.5 kDa protein bovine pancreatic trypsin inhibitor (BPTI). The results of the model-free analysis are also compared with the results obtained with the widely used HK function. Although we focus on the longitudinal relaxation rate R_1 here, the model-free approach can, of course, also be applied to R_2 data (which, however, rarely are used in NMRD work).

To adequately characterize a significantly stretched dispersion, the relaxation rate must be measured over at least 3 decades in frequency. This can currently be achieved only with fast field-cycling (FFC) techniques (*2*), possibly in combination with conventional measurements (*3*). The vast majority of NMRD data reported to date are FFC studies of water ^{1}H relaxation in aqueous biopolymer samples. For isotropic systems, such as protein solutions, the longitudinal ^{1}H relaxation rate due to fluctuating magnetic dipole–dipole couplings can be expressed as (*1, 54*)

$$R_1(\omega_0) = \alpha + \beta\{(1 - x)[0.2j(\omega_0) + 0.8j(2\omega_0)] + x[0.1j(0) + 0.3j(\omega_0) + 0.6j(2\omega_0)]\}, \quad [39]$$

where α is the part of R_1 that remains in the extreme-motional-narrowing regime up to the highest sampled frequency. Here we have also introduced the reduced SDF $j(\omega) = J(\omega)/C(0)$, so the parameter β is proportional to the mean-square fluctuation $C(0)$. Furthermore, x denotes the fraction of $C(0)$ that is due to dipole couplings with protons that do not contribute to the observed resonance ("unlike" spins). The effect of cross-relaxation (with "unlike" spins) on the measured R_1 is negligible in protein solutions (*54*) and is therefore ignored here.

TABLE 1
Convergence of Model-Free Analysis of Synthetic Data

N	χ_r^2	$P(N)$	α (s^{-1})	β (10^8 s^{-2})	$\langle\tau_C\rangle$ (ns)
1	56	—	0.692	3.11	15.1
2	3.3	1.000	0.609	4.52	12.0
3	1.10	0.997	0.582	5.11	10.8
4	1.12	0.570	0.581	5.15	10.8

We shall also analyze the dispersion data with the (inconsistent) HK function, expressed on the conventional form

$$R_1(\omega_0) = \alpha + \beta\tau_0 \,\mathrm{Re}\left[\frac{1}{1 + (i\sqrt{3}\omega_0\tau_0)^\kappa}\right]. \quad [40]$$

In the original notation of Hallenga and Koenig (*9*), $\alpha = 1/T_{1W} + D$, $\beta\tau_0 = A$, $\tau_0 = 1/(2\pi\sqrt{3}\,\nu_C)$, and $\kappa = \beta/2$. (The HK exponent β should not be confused with our mean-square fluctuation parameter β.) For the purpose of quantitatively comparing the HK and model-free approaches, we set $x = 0$ in Eq. [39], which then is virtually indistinguishable from (*6*)

$$R_1(\omega_0) = \alpha + \beta\, j(\sqrt{3}\,\omega_0). \quad [41]$$

For the model-free analysis of experimental data, however, we retain the full expression [39] and set $x = 1/3$, as found for water ^{1}H relaxation in BPTI solutions (*54*). (The full Eq. [39] can also be rather accurately approximated by Eq. [41], but with slightly redefined parameters (*54*).)

Synthetic Data

The convergence, robustness, and accuracy of the model-free approach has been tested against a range of synthetic data sets. The results of a typical validation test are shown in Fig. 2a and in Tables 1–3. The dispersion comprises 30 R_1 values evenly spaced on a logarithmic frequency axis and generated with the aid of Eqs. [33] and [39]. The mean error in R_1 is 2%. Seven Lorentzian terms were included with the τ_n values approximately logarithmically spaced in the range 3–200 ns and with the weights adjusted to make $c_n\tau_n$ the same for all 7 terms. The proportionality constant linking β and $C(0)$ was set to a value representative of water ^{1}H relaxation in a concentrated protein solution. The errors in the model-free parameters were determined from 1000 Monte Carlo realizations and are quoted at a confidence level of 68.3% (one standard deviation).

Figure 2a shows the optimal representation of the data, based on 3 Lorentzians. A fourth Lorentzian was rejected by the F test (see Table 1). The drastic reduction of the probability

TABLE 2
Robustness of Model-Free Analysis of Synthetic Data

m^a	N	χ_r^2	$P(N)$	$P(N+1)$	α (s^{-1})	β (10^8 s^{-2})	$\langle\tau_C\rangle$ (ns)
0	3	1.10	0.997	0.570	0.58 ± 0.01	5.1 ± 0.2	10.8 ± 0.3
1	3	1.11	0.997	0.579	0.58 ± 0.01	5.2 ± 0.2	10.6 ± 0.4
2	3	1.15	0.995	0.521	0.57 ± 0.02	5.3 ± 0.2	10.4 ± 0.5
3	3	1.14	0.981	0.571	0.60 ± 0.02	4.9 ± 0.3	11.1 ± 0.6
4	3	1.16	0.970	0.496	0.56 ± 0.04	5.4 ± 0.4	10.2 ± 0.7
5	3	1.28	0.872	0.619	0.66 ± 0.04	4.4 ± 0.2	12.4 ± 0.7
6	2	1.28	1.000	0.710	0.86 ± 0.03	3.2 ± 0.1	16.5 ± 0.6
6[b]	3	1.04	0.962	0.568	0.60 ± 0.01	4.7 ± 0.2	11.8 ± 0.4
10[c]	3	1.03	0.983	0.494	0.58 ± 0.01	5.1 ± 0.2	10.4 ± 0.5

[a] Number of data points omitted from the high-frequency end of the dispersion.
[b] Highest-frequency point retained.
[c] Data points omitted from the low-frequency end of the dispersion.

$P(N)$, here from 0.997 for the optimal 3-Lorentzian representation to 0.570 for $N = 4$, is typical. The choice of cutoff probability P_0 is therefore not critical. We recommend a value in the range 0.8–0.9; rare borderline cases should be examined individually. The model-free parameters converge rapidly to their final values and are stable when one more Lorentzian is added to the optimal representation (see Table 1).

Since experimental dispersion data are typically more or less logarithmically spaced, the integral of the dispersion profile is most sensitive to the quality of the high-frequency points. Inaccurate results can be expected if a high-frequency plateau is not evident in the data. To investigate the robustness of the method in this regard, we successively removed data points from the high-frequency end of the dispersion. For the data in Fig. 2, 4 points can be removed without much effect on the model-free parameters (see Table 2). When 6 points have been removed, the optimal representation becomes bi-Lorentzian and the parameter values change substantially. However, if the highest-frequency point is retained and the following 6 points are removed, the model-free parameters are within 10% of the results obtained with all 30 points. The low-frequency points are even less critical; removing the 10 lowest-frequency points hardly affects the model-free parameters at all.

TABLE 3
Accuracy of Model-Free and Hallenga–Koenig Analysis of Synthetic Data

Parameter	True value	Model-free	Hallenga–Koenig
χ_r^2	—	1.10 ($N = 3$)	2.92
α (s^{-1})	0.592	0.58 ± 0.01	0.43 ± 0.01
β (10^8 s^{-2})	5.00	5.1 ± 0.2	2.3 ± 0.1
$\langle\tau_C\rangle$ (ns)	11.2	10.8 ± 0.3	—
τ_0 (ns)	27.3	25.6 ± 1.0	25.2 ± 0.7
κ	—	—	0.69 ± 0.01
λ_-	0.607	0.55 ± 0.05	—
λ_+	0.695	0.66 ± 0.03	—

Table 3 shows that the model-free parameters can be accurately determined from dispersion data with 2% random error. Since the data were generated with $x = 1/3$ in Eq. [39] (as expected for water ^{1}H relaxation in protein solutions (*54*)) while $x = 0$ was used for the fits (to allow a direct comparison with the HK fit), the true values of the model-free parameters were determined from a separate multi-Lorentzian fit (with $x = 0$) to a synthetic data set generated with the same $\{c_n,\tau_n\}$ parameters but with negligible "measurement error."

The fit of the HK dispersion function [40] to the same synthetic data set is shown in Fig. 2b. As expected, this 4-parameter function does not fit the data as well as the 7-parameter function employed in the model-free analysis. This is reflected in the systematic variation of the residuals and in the larger reduced chi-square. More importantly, the α and β parameter values are substantially in error (see Table 3). The best determined parameter is τ_0, which in both approaches simply defines the frequency of half amplitude but does not have a simple physical interpretation. Since τ_0 exceeds the well-defined mean correlation time $\langle\tau_C\rangle$ to an extent (here, a factor 2.3) that depends on how stretched the dispersion is, the common practice (*4*, *9*, *11*, *12*, *15*, *16*, *18–22*, *28*, *29*) of identifying τ_0 with a macromolecular tumbling time is questionable. Moreover, when the prefactor (usually denoted by A) of the dispersive term in Eq. [40] is divided by τ_0 to obtain a static quantity (here denoted by β) proportional to the mean-square fluctuation, a correspondingly large systematic error is introduced in β. We emphasize that this is not merely a question of how to define a characteristic time in a useful manner. The prefactor measures the zero-frequency SDF $J(0) = C(0)\,\langle\tau_C\rangle$. If this quantity is divided by τ_0 rather than by $\langle\tau_C\rangle$, one clearly does not obtain the mean-square fluctuation $C(0)$, as generally assumed. For the synthetic data in Fig. 2, the HK analysis thus underestimates the true β by more than a factor 2. Since the microscopic interpretation of the β parameter has been clarified only recently (*3*, *5*, *55*), the systematic underestimation of β by the HK approach has gone unnoticed.

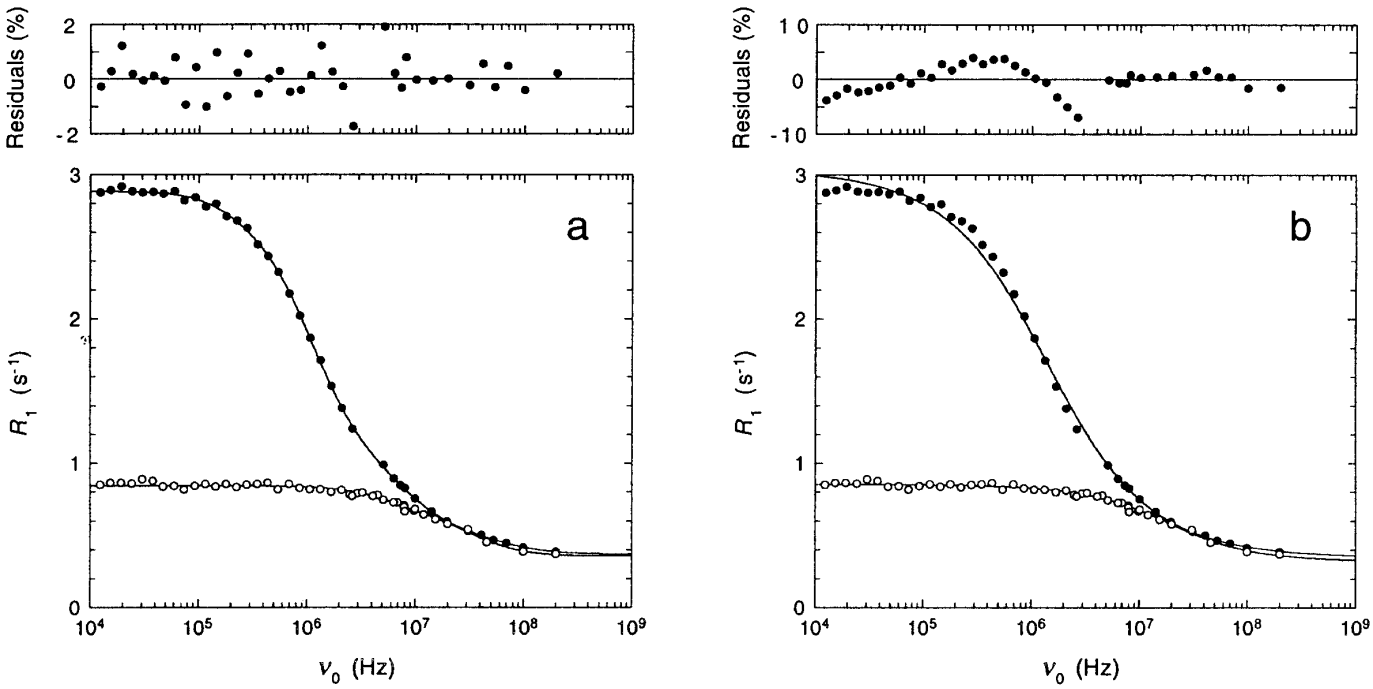

FIG. 3. Dispersion of the water ^{1}H longitudinal relaxation rate R_1 in aqueous solutions of 10 weight% BPTI at pH 4.5 and 300 K without any added salt (or buffer) (○) and after addition of 0.7 *M* NaCl (●). The relaxation rates were measured on a FFC instrument (Stelar) in the range 12 kHz–8 MHz and on conventional tunable and fixed-field spectrometers in the range 7–200 MHz. The BPTI was obtained from Novo Nordisk A/S (Gentofte, Denmark) and was exhaustively dialyzed to remove any salt. Protein solutions were made by dissolving the lyophilized protein in doubly distilled H_2O and the added NaCl was of >99.5% purity (Merck). The dispersion data were analyzed with the model-free approach (a) and the HK approach (b). Note the 5-fold scale difference between the residuals panels.

Any dispersion that can be expressed as a sum of Lorentzians, and this includes virtually all cases of interest, varies as $1 - \text{const}\ \omega_0^2$ and $\sim\omega_0^{-2}$ at low and high frequencies, respectively. The HK dispersion (with $\kappa < 1$) has a much weaker frequency dependence in both of these limits: $1 - \text{const}\ \omega_0^{\kappa}$ and $\sim\omega_0^{-\kappa}$, respectively. The HK function therefore has difficulty in reproducing the low- and high-frequency plateaus of a stretched dispersion (see Fig. 2b). In the many previous applications of this function, this deficiency has usually not been evident since the (mostly FFC) data rarely extend to sufficiently high frequencies to see the high-frequency plateau and often show considerable scatter at the lowest frequencies. (^{1}H dispersions from tissue do not even exhibit a low-frequency plateau.) The high-frequency slope of the HK function seen in Fig. 2b is responsible for the divergence of the dispersion integral and also causes the parameter α to be underestimated (here, by 25%) and the product $\beta\tau_0$ to be overestimated.

Experimental Data

The water ^{1}H dispersion from an aqueous solution of ca. 10 weight% BPTI is Lorentzian or nearly so (*54*). Under salt-free conditions, it has been established that the dispersion is due to 4 buried water molecules and a few labile BPTI protons (at pH 4.5, where the labile-proton contribution is minimal) (*54*). These water and BPTI protons exchange with the directly observed bulk water proton pool on a submillisecond timescale, but reside on the protein long enough (>10 ns) to sense its rotational motion. A quantitative analysis shows that these protons can account for the value of the β parameter deduced from the dispersion fit (*54*). The (mean) correlation time $\langle\tau_C\rangle$ is also close to the expected rotational correlation time of the protein under the experimental conditions.

Addition of salt to the protein solution has a dramatic effect on the dispersion profile, as illustrated in Fig. 3 for BPTI in 0.7 *M* NaCl. The dispersion not only increases 5-fold in magnitude but also becomes highly stretched, extending to much lower frequencies. The dramatic salt effect is undoubtedly due to protein–protein interactions, but neither the precise nature of these interactions, nor their dynamic consequences, is fully understood at present. (The salt effect exhibits a high degree of ion specificity, to be discussed elsewhere.) It has long been recognized that the water relaxation dispersion is a sensitive indicator of protein–protein interactions and several previous ^{1}H NMRD studies have focused on this aspect (*15, 16, 18, 21, 22, 56, 57*). The first step in analyzing dispersion data from strongly interacting protein solutions should be to establish whether the effects are purely dynamic or if structural changes are also involved. For example, can the salt effect in Fig. 3 be

TABLE 4
Convergence of Model-Free Analysis of Water ^{1}H NMRD Data for BPTI in 0.7 *M* NaCl

N	χ_r^2	*P(N)*	α (s^{-1})	β (10^8 s^{-2})	$\langle\tau_C\rangle$ (ns)
1	310	—	0.392	0.67	31.7
2	16	1.000	0.319	1.13	22.0
3	2.4	1.000	0.289	1.60	16.0
4	0.70	1.000	0.284	1.69	15.4
5	0.75	0.500	0.284	1.69	15.4

entirely attributed to slower protein tumbling or is part of the effect due to a larger β, e.g., from water molecules trapped between associating protein molecules? Ambiguities of this kind can be neatly resolved by a model-free analysis.

The results of a model-free analysis of the ^{1}H dispersion from BPTI in 0.7 *M* NaCl are shown in Fig. 3a and in Tables 4–6. The curve in Fig. 3a is the optimal representation of the 38 R_1 points (1% mean error). Four Lorentzian terms are required and the convergence of the parameters is excellent (see Table 4). The analysis is also robust; for example, the parameter values are not significantly affected if the two highest-frequency points are omitted. The HK fit, shown in Fig. 3b, is comparatively poor, as reflected in the 10-fold larger reduced chi-square and the systematic variation of the residuals (note the 5-fold difference of scale between Figs. 3a and 3b). Due to the extensive stretching of the dispersion profile, τ_0 is more than 4 times longer than $\langle\tau_C\rangle$. Consequently, the static β parameter comes out a factor 4 too small in the HK analysis (see Table 5). The salt-free dispersion is not far from Lorentzian (but the optimal representation is bi-Lorentzian) and, therefore, the two methods of analysis produce similar results (see Table 6).

What does this analysis say about the origin of the salt effect? The model-free analysis tells us that salt-induced protein–protein interactions produce a substantial slowing down of protein tumbling, with a 4-fold increase of the mean correlation time $\langle\tau_C\rangle$ and the large (asymmetric) dispersion stretching indicates association beyond the oligomer level. The structure of the individual protein molecules, however, appears to undergo little change in the association process since β varies by less than 40%. The HK analysis, if accepted, would imply an even larger dynamic effect (τ_0 increases by a factor 13), but would also suggest a substantial modification of the protein structure (perhaps a partial unfolding that exposes the previously buried water molecules) since the (apparent) β parameter decreases by a factor 2.6 on addition of salt (as opposed to the modest 40% increase obtained from the model-free analysis). This *qualitative* discrepancy clearly illustrates the pitfalls of the empirical approach that has been used in nearly all water ^{1}H NMRD studies since 1976.

CONCLUDING REMARKS

We have demonstrated here that the widely used HK dispersion function is physically inconsistent. Despite claims to the contrary, it is not the NMR analogue of the dielectric Cole–Cole dispersion and it does not satisfy the Kramers–Kronig relation. Moreover, the HK parameters do not have the physical significance that is generally ascribed to them. As shown by the example of BPTI in 0.7 *M* NaCl, the mean rotational correlation time and the mean-square fluctuation can each differ by more than a factor 4 from the corresponding HK parameters (τ_0 and A/τ_0). The HK function should therefore not be used to analyze NMRD data.

The model-free approach introduced here for the analysis of stretched dispersion profiles does not suffer from the limitations of empirical approaches and multi-parameter models (of uncertain validity). If the dispersion data are of reasonably high quality, the model-free analysis provides the mean-square fluctuation amplitude $C(0)$ (proportional to β), a purely static quantity, the mean correlation time $\langle\tau_C\rangle$, and one or more shape parameters. The model-free parameters have well-defined physical significance and allow the static and dynamic information content of the dispersion profile to be separated, as for a Lorentzian dispersion. The model-free approach was validated with the aid of synthetic data and was shown to be robust and accurate.

The physical mechanism responsible for stretching of water ^{1}H dispersion profiles in biological systems has not yet been unambiguously established. Several mechanisms are possible (*3*). If some of the buried water molecules that contribute to the dispersion have residence times τ_W comparable to the rotational correlation time τ_R of the protein, then the effective correlation time τ_C is given by $1/\tau_C = 1/\tau_R + 1/\tau_W$. A τ_W distribution can therefore produce a high-frequency tail in the dispersion profile even if the protein undergoes free symmetric-top rotational diffusion. This mechanism is probably relatively unimportant and cannot account for the common observation of stretching to lower frequencies with a concomitant increase of the dispersion magnitude. Likewise, effects of

TABLE 5
Accuracy of Model-Free and Hallenga–Koenig Analysis of Water ^{1}H NMRD Data for BPTI in 0.7 *M* NaCl

Parameter	Model-free $x = 1/3$	Model-free $x = 0$	Hallenga–Koenig
χ_r^2	0.7	0.7	7.3
α (s^{-1})	0.284 ± 0.003	0.371 ± 0.003	0.345 ± 0.002
β (10^8 s^{-2})	1.69 ± 0.06	1.68 ± 0.06	0.414 ± 0.004
$\langle\tau_C\rangle$ (ns)	15.4 ± 0.5	15.0 ± 0.5	—
τ_0 (ns)	64.4 ± 0.7	62.4 ± 0.7	65.1 ± 0.9
κ	—	—	0.677 ± 0.005
λ_-	0.34 ± 0.02	0.35 ± 0.02	—
λ_+	0.77 ± 0.01	0.77 ± 0.01	—

TABLE 6
Salt Effect on Water ^{1}H Dispersion in BPTI Solution: Model-Free versus Hallenga–Koenig Analysis

	Model-free ($x = 0$)		Hallenga–Koenig	
Parameter	No salt	0.7 *M* NaCl	No salt	0.7 *M* NaCl
χ_r^2	1.8	0.7	1.8	7.3
α (s^{-1})	0.355 ± 0.004	0.371 ± 0.003	0.321 ± 0.007	0.345 ± 0.002
β (10^8 s^{-2})	1.22 ± 0.06	1.68 ± 0.06	1.08 ± 0.05	0.414 ± 0.004
$\langle\tau_C\rangle$ (ns)	4.0 ± 0.2	15.0 ± 0.5	—	—
τ_0 (ns)	5.1 ± 0.2	62.4 ± 0.7	4.9 ± 0.2	65.1 ± 0.9

asymmetric-top rotational diffusion should be undetectably small for most globular proteins. A residence time distribution can also produce dispersion stretching when the residence times are comparable to the intrinsic relaxation times. This mechanism should be most important for labile protein protons, which may dominate the water ^{1}H dispersion (*54, 58*). In semisolid protein–water systems, such as gels, chemically cross-linked proteins, and tissues, the proteins are not free to reorient and the dispersion is then governed by proton (and water) exchange dynamics. Since the exchange rates span a wide range, the observed relaxation rate is dominated by protons with exchange rates comparable to the dipolar coupling frequency (*59*). A distribution of (intermolecular) dipole couplings then leads to dispersion stretching. This should be a major effect in semisolid aqueous systems. In concentrated protein solutions, the principal mechanism of dispersion stretching is undoubtedly protein–protein interactions. NMRD data contain valuable information about such interactions and the model-free approach advocated here allows their dynamic and structural consequences to be disentangled.

ACKNOWLEDGMENTS

We are grateful to Novo Nordisk A/S for a generous gift of BPTI. This work was supported by grants from the Crafoord Foundation and the Swedish Natural Science Research Council (NFR).

REFERENCES

1. A. Abragam, "The Principles of Nuclear Magnetism," Clarendon, Oxford (1961).
2. F. Noack, *Prog. NMR Spectrosc.* **18,** 171 (1986).
3. B. Halle, V. P. Denisov, and K. Venu, *in* "Modern Techniques in Protein NMR" (L. J. Berliner and N. R. Krishna, Eds.), Vol. 17, Plenum, New York (1998).
4. S. H. Koenig and R. D. Brown, *Progr. NMR Spectrosc.* **22,** 487 (1991).
5. V. P. Denisov and B. Halle, *Faraday Discuss.* **103,** 227 (1996).
6. S. H. Koenig and W. E. Schillinger, *J. Biol. Chem.* **244,** 3283 (1969).
7. B. Blicharska, Z. Florkowski, J. W. Hennel, G. Held, and F. Noack, *Biochim. Biophys. Acta* **207,** 381 (1970).
8. R. Kimmich and F. Noack, *Z. Naturforsch. A* **25,** 299 (1970).
9. K. Hallenga and S. H. Koenig, *Biochemistry* **15,** 4255 (1976).
10. S. H. Koenig, R. G. Bryant, K. Hallenga, and G. S. Jacob, *Biochemistry* **17,** 4348 (1978).
11. S. H. Koenig, *in* "Water in Polymers" (S. P. Rowland, Eds.), Vol. 127, p. 157, Am. Chem. Soc., Washington, DC (1980).
12. S. H. Koenig, R. D. Brown, I. Bertini, and C. Luchinat, *Biophys. J.* **41,** 179 (1983).
13. S. H. Koenig, R. D. Brown, D. Adams, D. Emerson, and C. G. Harrison, *Invest. Radiol.* **19,** 76 (1984).
14. S. H. Koenig and R. D. Brown, *Magn. Reson. Med.* **1,** 437 (1984).
15. S. Conti, *Molec. Phys.* **59,** 449 (1986).
16. S. Conti, *Molec. Phys.* **59,** 483 (1986).
17. S. H. Koenig and R. D. Brown, *in* "NMR Spectroscopy of Cells and Organisms" (R. K. Gupta, Ed.), Vol. 2, p. 75, CRC Press, Boca Raton, FL (1987).
18. H. H. Raeymaekers, H. Eisendrath, A. Verbeken, Y. Van Haverbeke, and R. N. Muller, *J. Magn. Reson.* **85,** 421 (1989).
19. I. Bertini, C. Luchinat, R. D. Brown, and S. H. Koenig, *J. Am. Chem. Soc.* **111,** 3532 (1989).
20. I. Bertini, C. Luchinat, M. S. Viezzoli, L. Banci, S. H. Koenig, H. T. Leung, and J. E. Coleman, *Inorg. Chem.* **28,** 352 (1989).
21. S. H. Koenig, C. F. Beaulieu, R. D. Brown, and M. Spiller, *Biophys. J.* **57,** 461 (1990).
22. S. H. Koenig, R. D. Brown, M. Spiller, B. Chakrabarti, and A. Pande, *Biophys. J.* **61,** 776 (1992).
23. S. H. Koenig, R. D. Brown, and R. Ugolini, *Magn. Reson. Med.* **29,** 77 (1993).
24. S. H. Koenig and R. D. Brown, *Magn. Reson. Med.* **30,** 685 (1993).
25. S. H. Koenig, *Biophys. J.* **69,** 593 (1995).
26. S. H. Koenig, *in* "Encyclopedia of Nuclear Magnetic Resonance" (D. M. Grant and R. K. Harris, Eds.), p. 1819, Wiley, New York (1995).
27. S. H. Koenig and R. D. Brown, *in* "Encyclopedia of Nuclear Magnetic Resonance" (D. M. Grant and R. K. Harris, Eds.), p. 4108, Wiley, New York (1995).
28. P. Roose, J. van Craen, R. Finsy, and H. Eisendrath, *J. Magn. Reson. A* **115,** 20 (1995).
29. D. Zhou and R. G. Bryant, *J. Biomol. NMR* **8,** 77 (1996).
30. B. Halle and H. Wennerström, *J. Magn. Reson.* **44,** 89 (1981).
31. L. Werbelow and R. E. London, *Concepts Magn. Reson.* **8,** 325 (1996).
32. K. W. Wagner, *Ann. Phys.* **40,** 817 (1913).
33. W. A. Yager, *Physics* **7,** 434 (1936).
34. L. D. Landau and E. M. Lifshitz, "Statistical Physics," Pergamon, Oxford (1980).
35. J. McConnell, "Rotational Brownian Motion and Dielectric Theory," Academic Press, London (1980).

36. P. Debye, "Polar Molecules," Chemical Catalogue Co., New York (1929).

37. K. S. Cole and R. H. Cole, *J. Chem. Phys.* **9,** 341 (1941).

38. R. M. Fuoss and J. G. Kirkwood, *J. Am. Chem. Soc.* **63,** 385 (1941).

39. H. S. Gutowsky, A. Saika, M. Takeda, and D. E. Woessner, *J. Chem. Phys.* **27,** 534 (1957).

40. A. Odajima, *Progr. Theoret. Phys. (Kyoto) Suppl.* **10,** 142 (1959).

41. H. A. Resing, J. K. Thompson, and J. J. Krebs, *J. Phys. Chem.* **68,** 1621 (1964).

42. T. M. Connor, *Trans. Faraday Soc.* **60,** 1574 (1964).

43. G. J. Krüger and G. A. Helcké, *in* "Magnetic Resonance and Relaxation" (R. Blinc, Ed.), p. 1136, North-Holland, Amsterdam (1967).

44. H. A. Resing, *Adv. Mol. Relax. Proc.* **1,** 109 (1968).

45. L. J. Lynch and D. S. Webster, *J. Polymer Sci. Symp.* **49,** 43 (1975).

46. M. Rydzy, *Acta Phys. Polon. A* **58,** 853 (1980).

47. N. G. van Kampen, "Stochastic Processes in Physics and Chemistry," North-Holland, Amsterdam (1981).

48. L. D. Favro, *Phys. Rev.* **119,** 53 (1960).

49. A. Ferrarini, P. L. Nordio, and G. J. Moro, *in* "The Molecular Dynamics of Liquid Crystals" (G. R. Luckhurst and C. A. Veracini, Eds.), p. 41, Kluwer Academic, Dordrecht (1994).

50. B. Halle, *J. Chem. Phys.* **94,** 3150 (1991).

51. J. H. Freed, *J. Chem. Phys.* **66,** 4183 (1977).

52. W. H. Press, B. P. Flannery, S. A. Teukolsky, and W. T. Vetterling, "Numerical Recipes. The Art of Scientific Computing," Cambridge Univ. Press, Cambridge (1986).

53. D. N. Rutledge (Ed.), "Signal Treatment and Signal Analysis in NMR," Elsevier, Amsterdam (1996).

54. K. Venu, V. P. Denisov, and B. Halle, *J. Am. Chem. Soc.* **119,** 3122 (1997).

55. V. P. Denisov and B. Halle, *J. Mol. Biol.* **245,** 682 (1995).

56. T. R. Lindstrom and S. H. Koenig, *J. Magn. Reson.* **15,** 344 (1974).

57. T. R. Lindstrom, S. H. Koenig, T. Boussios, and J. F. Bertles, *Biophys. J.* **16,** 679 (1976).

58. V. P. Denisov, G. Carlström, K. Venu, and B. Halle, *J. Mol. Biol.* **268,** 118 (1997).

59. B. Halle and V. P. Denisov, *Biophys. J.* **69,** 242 (1995).